A&A 586, A160 (2016)
DOI: 10.1051/0004-6361/201527235

Astronomy & Astrophysics

The role of binaries in the enrichment of the early Galactic halo

II. Carbon-enhanced metal-poor stars: CEMP-no stars

T. T. Hansen[1], J. Andersen[2,3], B. Nordström[2,3], T. C. Beers[4], V. M. Placco[4], J. Yoon[4], and L. A. Buchhave[5,6]

[1] Landessternwarte, ZAH, Heidelberg University, Königstuhl 12, 69117 Heidelberg, Germany
e-mail: thansen@lsw.uni-heidelberg.de
[2] Dark Cosmology Centre, The Niels Bohr Institute, University of Copenhagen, Juliane Maries Vej 30, 2100 Copenhagen, Denmark
[3] Stellar Astrophysics Centre, Department of Physics and Astronomy, Aarhus University, 8000 Aarhus C, Denmark
[4] Department of Physics and JINA Center for the Evolution of the Elements, University of Notre Dame, Notre Dame, IN 46556, USA
[5] Harvard-Smithsonian Center for Astrophysics, Cambridge, MA 02138, USA
[6] Centre for Star and Planet Formation, University of Copenhagen, 1350 Copenhagen, Denmark

Received 24 August 2015 / Accepted 19 November 2015

ABSTRACT

Context. The detailed composition of most metal-poor halo stars has been found to be very uniform. However, a fraction of 20–70% (increasing with decreasing metallicity) exhibit dramatic enhancements in their abundances of carbon; these are the so-called carbon-enhanced metal-poor (CEMP) stars. A key question for Galactic chemical evolution models is whether this non-standard composition reflects that of the stellar natal clouds or is due to local, post-birth mass transfer of chemically processed material from a binary companion; CEMP stars should then all be members of binary systems.

Aims. Our aim is to determine the frequency and orbital parameters of binaries among CEMP stars with and without over-abundances of neutron-capture elements – CEMP-*s* and CEMP-no stars, respectively – as a test of this local mass-transfer scenario. This paper discusses a sample of 24 CEMP-no stars, while a subsequent paper will consider a similar sample of CEMP-*s* stars.

Methods. High-resolution, low S/N spectra of the stars were obtained at roughly monthly intervals over a time span of up to eight years with the FIES spectrograph at the Nordic Optical Telescope. Radial velocities of ∼100 m s^{-1} precision were determined by cross-correlation after each observing night, allowing immediate, systematic follow-up of any variable object.

Results. Most programme stars exhibit no statistically significant radial-velocity variation over this period and appear to be single, while four are found to be binaries with orbital periods of 300–2000 days and normal eccentricity; the binary frequency for the sample is 17 ± 9%. The single stars mostly belong to the recently identified low-C band, while the binaries have higher absolute carbon abundances.

Conclusions. We conclude that the nucleosynthetic process responsible for the strong carbon excess in these ancient stars is unrelated to their binary status; the carbon was imprinted on their natal molecular clouds in the early Galactic interstellar medium (ISM) by an even earlier external source, strongly indicating that the CEMP-no stars are likely bona fide second-generation stars. We discuss potential production sites for carbon and its transfer across interstellar distances in the early ISM, and the implications for the composition of high-redshift DLA systems.

Key words. Galaxy: formation – Galaxy: halo – stars: chemically peculiar – binaries: spectroscopic – ISM: structure

1. Introduction

Over the past few decades, the collective effort of large-scale spectroscopic surveys to identify and analyse very metal-poor (VMP; [Fe/H] < −2.0) and extremely metal-poor (EMP; [Fe/H] < −3.0) stars in the halo system of the Milky Way have provided an increasingly detailed picture of the star-to-star elemental-abundance variations that constrain the early chemical evolution of the Galaxy (Cayrel et al. 2004; Bonifacio et al. 2009); for general reviews, see Beers & Christlieb (2005), Ivezic et al. (2012), Frebel & Norris (2015).

However, chemically peculiar stars exist, the abundance patterns of which deviate markedly from those of the bulk of Population II stars. Identifying the nature and origin of these stars should enable identification of their progenitors and lead to a better understanding of the processes of nucleosynthesis and mass ejection that are responsible for the production of their distinctive chemical signatures. This information will constrain the nature of the very first generations of stars prior to the dilution of these signatures by later mixing with the interstellar medium (ISM) of the Galaxy, which ultimately establishes the mean abundance trends for relatively more metal-rich stars.

A key element in this context is carbon, the first heavy element synthesised after the Big Bang and found with increasing frequency in very metal-poor stars. Carbon-enhanced metal-poor (CEMP) stars were originally identified among the VMP and EMP stars discovered in the HK survey of Beers, Preston, & Shectman (Beers et al. 1985, 1992), and supplemented by a number of surveys since. The fraction of CEMP stars rises with decreasing iron abundance, [Fe/H] (the conventional metallicity indicator), which makes them particularly important for studies of the very first stages of the formation and evolution of the Galactic halo.

The CEMP stars comprise a number of different subclasses (initially defined by Beers & Christlieb 2005). The CEMP subclasses with the most members are

(i) The CEMP-*s* stars (indicating the presence of *s*-process elements in addition to the carbon enhancement; [C/Fe] > +0.7 and [Ba/Fe] > +1.0), the vast majority of which can be

accounted for by scenarios involving the transfer of enriched material from a binary companion that has passed through the asymptotic giant branch (AGB) stage of evolution[1], and

(ii) The CEMP-no stars (indicating carbon enrichment, but no enhancement in neutron-capture elements; [C/Fe] > +0.7 and [Ba/Fe] < 0.0), the origin of which has still not been identified with certainty. A number of lines of evidence (described in detail below) strongly suggest association of the CEMP-no stars with the nucleosynthesis products of the very first stars born in the Universe, i.e. that they are bona fide second-generation stars.

Aoki et al. (2002a) and Ryan et al. (2005) first called attention to the apparent contrast in the heavy-element abundance patterns among several subclasses of CEMP stars and speculated about their likely origin. In particular, Ryan et al. (2005) predicted that the binary fraction of the CEMP-no stars should be the same as for non-carbon-enhanced, metal-poor stars, if they acquired their carbon from the explosions of previous-generation massive stars. Moreover, Carollo et al. (2012, 2014) found the bulk of CEMP stars in the outer halo to be CEMP-no stars, while the CEMP-*s* stars appear to be predominantly associated with the inner halo, a finding of substantial-if as yet unclear-significance for our understanding of the formation of the haloes of galaxies, including our own.

The present series of papers considers the origin of chemically peculiar stars at very low metallicity, and tests whether their distinctive abundance signatures can be accounted for by alteration of their birth chemistry by an evolved binary companion, based on an eight-year programme of systematic, precise radial-velocity monitoring for larger samples of chemically peculiar stars than have heretofore been studied in this way. What sets this entire project apart from earlier studies is our emphasis on high precision, the homogeneity of the data over a time span compatible with the periods of likely binaries in the sample, and our systematic follow-up of any suspected variable objects in the sample. This enables us to identify single and binary stars on a rigorous, objective star-by-star basis.

Hansen et al. (2011) first showed that the enhancement of *r*-process elements observed in a small fraction (3–5%) of VMP and EMP stars is not causally connected to membership in a binary system, a conclusion that was confirmed and further strengthened in Paper I of this series (Hansen et al. 2015b). The present paper examines the same question for the class of CEMP-no stars, based on similarly precise and systematic radial-velocity monitoring. Paper III of this series (Hansen et al. 2015c) addresses the role that binaries play in the production of CEMP-*s* stars, using the same approach.

This paper is outlined as follows. Section 2 summarises our observing strategy and selection of programme stars, and briefly describes the observational techniques employed. The results are presented in Sect. 3. In Sect. 4, we discuss the constraints imposed by these results on the origin of CEMP-no stars and outline the current evidence that shows they can be identified with the first stars able to form in the early Galaxy and Universe. Brief conclusions and thoughts on what can be learned from future radial-velocity monitoring of CEMP-no stars are presented in Sect. 5.

[1] Even though progress is being made, the high fraction of CEMP-*s* stars found in the early Universe still poses a challenge for theoretical population synthesis modelling (e.g. Izzard et al. 2009; Abate et al. 2013, 2015).

2. Observing strategy, observations, and data analysis

2.1. Observing strategy for this project

Previous forays into this subject (e.g. Lucatello et al. 2005; Starkenburg et al. 2014) have typically comprised a limited number of radial-velocity observations over a limited time span, sometimes combined with a literature search for earlier data, usually small in number and necessarily heterogeneous in origin. A Monte Carlo simulation was then used to assess the likely frequency of typical binaries in the sample.

Our approach throughout this project is completely different and builds on the earlier examples of Duquennoy & Mayor (1991), Nordström et al. (1997), and Carney et al. (2003). We obtained a sufficient number of precise radial-velocity observations in a homogeneous system over a sufficiently long time span to detect any binaries in the sample, even if their orbital periods might be substantially longer than the time span of the observations (up to ∼2900 days in our case). Moreover, the observations were reduced promptly after each observing night in order to rapidly detect any incipient variability and to schedule follow-up observations as appropriate for each object, so the reality and origin of the variations could eventually be assessed with confidence.

As described in Paper I, this strategy enabled us to follow the star HE 1523−0901 over several orbital revolutions and to identify it as a very low-inclination binary, despite its period of 303 days (∼a year) and velocity semi-amplitude of only 0.35 km s^{-1}. Paper III demonstrate how it has also enabled us to detect several binaries with periods of a decade or much more, although we only followed them for ≲3000 days.

In such situations, the χ^2 statistic is a much more secure indicator of velocity variability for a given star than Monte Carlo simulations of variations in published data, although judgement must still be exercised in each case when reviewing the probability, $P(\chi^2)$, that a star is truly single. For example, the low-amplitude binary HE 1523−0901 has $P(\chi^2) < 10^{-6}$ (Paper I), while the CEMP-*s* star HE 0017−0055, classified as a long-period binary in Paper III, also exhibits an apparently similar, regular, short-period variation of period 385 days and amplitude 0.54 km s^{-1}, followed over 8 cycles. Even so, Jorissen et al. (2016) concluded, based on other evidence, that the short-period variations were due to pulsations rather than binary motion (see also the discussion of HE 1410+0213 below).

2.2. Sample selection

Our initial observing list, established in 2006, comprised a total of 23 CEMP stars with pedigrees of widely different quality and 17 *r*-process enhanced stars drawn from the HK surveys of Beers, Preston, & Shectman (Beers et al. 1985, 1992) and the Hamburg/ESO survey of Christlieb and collaborators (Christlieb et al. 2008). The initial sample of CEMP stars also included one of the most metal-poor stars known to date, HE 1327−2326, with [Fe/H] = −5.8 (Aoki et al. 2006; Frebel et al. 2006).

By 2010, the overall conclusion of the *r*-process programme had already become clear (Hansen et al. 2011), while the significance of the different spatial distributions of the CEMP-*s* and CEMP-no subclasses, and the potentially different binary frequencies and origins of their carbon excess, had assumed greater importance. At the same time, our observing technique had been refined and amply tested as described above. From 2011, the *r*-process programme was therefore limited to sparsely sampled

Table 1. Sample of CEMP-no stars monitored for radial-velocity variation.

Stellar ID	RA (J2000)	Dec (J2000)	V	$B-V$	Ref	[Fe/H]	[C/Fe]	[Ba/Fe]	Ref
HE 0020−1741	00:22:44	−17:24:28	12.89	0.94	a	−4.11	+1.36	<−0.67	1
CS 29527−015*	00:29:11	−19:10:07	14.26	0.40	d	−3.55	+1.18	<+0.10	10
CS 22166−016	00:58:24	−14:47:07	12.75	0.65	b	−2.40	+1.02	−0.37	4
HE 0219−1739	02:21:41	−17:25:37	14.73	1.52	b	−3.09	+1.90	<−1.39	1
BD+44°493	02:26:50	+44:57:47	9.22	0.67	a	−3.83	+1.35	−0.60	2
HE 0405−0526	04:07:47	−05:18:11	10.72	0.71	a	−2.18	+0.92	−0.22	1
HE 1012−1540*	10:14:53	−15:55:53	14.04	0.66	a	−3.51	+2.22	+0.19	6
HE 1133−0555	11:36:12	+06:11:43	15.43	0.64	b	−2.40	+2.20	−0.58	1
HE 1150−0428	11:53:07	−04:45:03	15.01	0.76	a	−3.21	+2.28	−0.44	6
HE 1201−1512	12:03:37	−15:29:33	13.79	0.55	a	−3.92	+1.60	<−0.34	3
HE 1300+0157	13:02:56	+01:41:52	14.06	0.48	b	−3.49	+1.31	−0.74	6
BS 16929−005	13:03:30	+33:51:09	13.61	0.62	b	−3.27	+0.99	−0.41	3
HE 1300−0641	13:03:34	−06:57:21	14.80	0.62	b	−3.14	+1.29	−0.77	8
HE 1302−0954	13:04:58	−10:10:11	13.96	0.79	a	−2.25	+1.17	<−0.53	1
CS 22877−001	13:13:55	−12:11:42	12.16	0.77	b	−2.71	+1.00	−0.49	5
HE 1327−2326*	13:30:06	−23:41:54	13.53	0.44	b	−5.76	+4.26	<+1.46	3
HE 1410+0213	14:13:06	+01:59:21	13.05	1.14	b	−2.14	+1.71	−0.26	6
HE 1506−0113	15:09:14	−01:24:57	14.44	0.64	a	−3.54	+1.65	−0.80	3
CS 22878−027	16:37:36	+10:22:08	14.41	0.44	c	−2.52	+0.86	<−0.75	3
CS 29498−043	21:03:52	−29:42:50	13.63	1.12	b	−3.75	+1.90	−0.45	7
CS 29502−092	22:22:36	−01:38:24	11.87	0.77	b	−2.99	+0.96	−1.20	3
HE 2318−1621	23:21:22	−16:05:06	12.73	0.68	a	−3.67	+1.04	−1.61	9
CS 22949−037	23:26:30	−02:39:58	14.36	0.79	b	−3.93	+1.01	−0.77	6
CS 22957−027	23:59:13	−03:53:49	13.62	0.80	b	−3.06	+2.13	−0.96	6

Notes. (*) Stars not formally qualifying as CEMP-no stars according to the [Ba/Fe] criterion. However, see discussion of their light-element abundance signatures in Sect. 2.3.

References. Photometry: (a) Henden et al. (2015); (b) Beers et al. (2007); (c) Preston et al. (1991); (d) Norris et al. (1999).
Abundances: (1) This work; (2) Ito et al. (2013); (3) Yong et al. (2013); (4) Giridhar et al. (2001); (5) Aoki et al. (2002a); (6) Cohen et al. (2013); (7) Aoki et al. (2002c); (8) Barklem et al. (2005); (9) Placco et al. (2014a); (10) Bonifacio et al. (2009) and M. Spite (priv. comm.).

long-term monitoring, while 25 likely new CEMP-no stars were selected from the same sources and added to the regular programme. We also included the bright CEMP-no star BD+44°493 in the programme, the abundance pattern of which has been studied extensively (Ito et al. 2013; Placco et al. 2014b). Ultimately, it turned out that two of the candidate CEMP-no stars were not sufficiently carbon enhanced to be considered CEMP stars and were dropped from our programme. In addition, one of our candidate CEMP-*s* stars, to be discussed in Paper III, turned out to be a CEMP-no star and hence was moved to the sample discussed here.

Our final sample of 24 CEMP-no programme stars is provided in Table 1, which lists their V magnitudes; $B-V$ colours; and reported [Fe/H], [C/Fe], and [Ba/Fe] abundances (either from the literature or determined as described below).

2.3. Abundance information for the sample stars

As seen from Table 1, many of our sample stars have detailed abundance information available from high-resolution spectroscopy obtained with 6−10 m telescopes (the "First Stars" project, e.g. Bonifacio et al. 2009, is a notable exception since that project deliberately avoided carbon-enhanced stars). On that background, the present project at the 2.5 m Nordic Optical Telescope (NOT) focused on establishing the binary status of known CEMP stars.

Only five of the stars in our sample had no Ba abundance measurement in the published literature; one star (HE 0405−0526) also lacked published estimates of [Fe/H] and [C/Fe]. For HE 0405−0526, we therefore derived estimates of [Fe/H] and [C/Fe] from a medium-resolution ($R \sim 2000$) spectrum obtained with the SOAR Telescope (program SO2011B-002), using the n-SSPP software pipeline described in detail by Beers et al. (2014). For this star, and for the remaining stars with initially missing Ba abundances, we used the high-resolution spectra obtained for the radial-velocity monitoring. These were co-added to produce a higher signal-to-noise ratio (S/N) spectrum, following the description in Paper I for co-adding templates, but including only the orders containing the Ba lines at $\lambda = 4554$ Å and $\lambda = 4934$ Å.

Barium abundances or upper limits were then obtained from spectral synthesis of these spectra, using the 2014 version of MOOG and the line list retrieved from VALD (the Vienna Atomic Line Database[2] Kupka et al. 1999), including hyperfine splitting and isotopic shifts. The Asplund et al. (2009) solar abundances were assumed. The co-added spectra may have slightly broadened lines due to the initial correlation when creating this spectrum, as described in Paper I, which could influence the abundances derived from these spectra and result in a higher abundance estimate. We have taken this into account when estimating the error on the derived abundances.

For three of the stars we considered, only an upper limit on the Ba abundance could be derived; however, all of these firmly classify the stars as CEMP-no stars. For HE 0405−0526 and HE 1133−0555, we derive Ba abundances of [Ba/Fe] = −0.22 and [Ba/Fe] = −0.58, respectively, with an estimated error of 0.3 dex, also classifying them as CEMP-no stars.

For the three stars CS 29527−015, HE 1012−1540, and HE 1327−2326, the derived Ba abundances or upper limits ([Ba/Fe] < +0.10, [Ba/Fe] = +0.19, and [Ba/Fe] < +1.46,

[2] http://vald.astro.univie.ac.at/~vald3/php/vald.php

Table 2. Results of radial-velocity monitoring.

Stellar ID	Nobs	Template	RV mean (km s^{-1})	σ (km s^{-1})	ΔT (Days)	$P(\chi^2)$	Binary
HE 0020−1741	9	Co-add	+9.039	0.212	1066	0.122	No
CS 29527−015	6	BD+44°493	+47.122	0.425	1064	0.992	No
CS 22166−016	8	Co-add	−210.504	0.803	1034	0.255	No
HE 0219−1739	15	Co-add	+106.689	5.090	2207	0.000	Yes
BD+44°493	18	Co-add	−150.084	0.051	1298	0.927*	No
HE 0405−0526	13	Co-add	+165.657	0.039	904	0.993	No
HE 1012−1540	8	HE 0405−0526	+226.052	0.207	802	0.988	No
HE 1133−0055	9	HE 0405−0526	+270.632	0.336	2217	0.707	No
HE 1150−0428	13	Strongest	+48.042	8.350	2220	0.000	Yes
HE 1201−1512	5	Delta	+239.450	1.854	42	0.582	No
HE 1300+0157	5	BD+44°493	+74.494	0.583	412	0.122*	No
BS 16929−005	7	Delta	−50.627	0.474	885	0.912*	No
HE 1300−0641	2	HE 0405−0526	+68.846	0.114	386	0.827	No
HE 1302−0954	3	BD+44°493	+32.538	0.039	386	0.968	No
CS 22877−001	15	Co-add	+166.297	0.111	2923	0.737*	No
HE 1327−2326	9	Delta	+64.343	1.170	2577	0.545	No
HE 1410+0213	23	Co-add	+81.140	0.180	3006	0.196	No
HE 1506−0113	10	Delta	−81.467	2.772	493	0.000*	Yes
CS 22878−027	7	Delta	−90.870	0.768	1034	0.775*	No
CS 29498−043	15	Delta	−32.488	0.701	2603	0.967	No
CS 29502−092	20	Co-add	−67.160	0.173	2603	0.616*	No
HE 2318−1621	7	BD+44°493	−41.698	0.279	1034	0.172	No
CS 22949−037	7	BD+44°493	−125.560	0.269	765	0.894*	No
CS 22957−027	18	Co-add	−67.305	5.736	1568	0.000	Yes

Notes. Columns: star name; number of NOT observations; template used; mean heliocentric radial velocity and standard deviation; time span; variability criterion $P(\chi^2)$; and binary status. (*) Additional literature data included in $P(\chi^2)$, see Sect. 3.2 and Table 3.

respectively) do not qualify them as CEMP-no stars, based on the formal definition ([Ba/Fe] < 0). However, enhancement of the light elements has also been found to be associated with the CEMP-no subclass; see the recent discussion by Norris et al. (2013b). For HE 1012−1540, Cohen et al. (2013) found [N/Fe] = +1.25, [O/Fe] = +2.14, [Na/Fe] = +1.02, and [Mg/Fe] = +1.38, while Frebel et al. (2008) derived [N/Fe] = +4.53, [O/Fe] = +3.68, [Na/Fe] = +2.17, and [Mg/Fe] = +1.67 for HE 1327−2326. Frebel et al. (2008) also obtained a relatively high Sr abundance for this star, [Sr/Fe] = +0.98. An absolute carbon abundance of A(C) = log ϵ(C) = 6.06 was reported for CS 29527−015 by Bonifacio et al. (2009), also pointing toward a CEMP-no classification for this star, but further observations are needed to confirm this.

2.4. Radial-velocity observations and data reduction

The observations, data reduction, and analysis procedures were those described in Paper I of this series, to which we refer the interested reader for details; only a brief summary is given here. Weather permitting, our programme stars were observed at roughly monthly intervals with the FIES spectrograph at the 2.5 m NOT on La Palma, Spain. The spectra cover a wavelength range of 3640 Å to 7360 Å at a resolving power of $R \sim 46\,000$, and have an average S/N of 10. For obvious reasons, the stars added to the programme in 2010 were observed for shorter spans and, coupled with adverse spring weather conditions, were observed less completely than stars from the initial sample.

Reductions and multi-order cross-correlation with a template spectrum were performed with software developed by L. Buchhave. The template spectrum used for a given star was the spectrum with maximum S/N ("strongest"); a co-added spectrum constructed from all the best spectra for the star ("Co-add"); a synthetic spectrum consisting of delta functions ("Delta"); or, finally, co-added spectra of the bright CEMP-no stars BD+44°493 or HE 0405−0526. The template used for each star is identified in Table 2.

Our error definitions and error analysis are also described in Paper I. We note especially that the standard deviations given in Tables 2 and 3 are the standard deviation of the radial velocity observations for each star, not standard errors of the mean.

The individual standard stars observed on this programme, along with their derived mean heliocentric radial velocities (RV) and standard deviations (σ), are listed in Table 2 of Paper I in this series; typical standard deviations are 40 m s^{-1} over a time span of ∼2800 days. The average difference of our mean velocities from the standard values is 73 m s^{-1} with a standard deviation of 69 m s^{-1}, demonstrating that our results are not limited by the stability of the FIES spectrograph.

3. Results

The results of our RV observations for our CEMP-no stars are summarised in Table 2, which lists the number of observations (Nobs), the cross-correlation templates employed, the mean heliocentric radial velocity (RV mean) and standard deviation (σ) over the time span covered by our own observations (ΔT), and the binary status of each programme star. The individual observed heliocentric radial velocities are listed in Appendix A together with the Julian dates of the observations and the corresponding internal errors.

As for the r-process-element enhanced stars discussed in Paper I, the external standard deviations of the observed velocities vary from <100 m s^{-1} for the bright targets, dominated by centring and guiding errors, to ∼1 km s^{-1} for the fainter and/or metal-poor targets with low S/N spectra.

Table 3. Additional data for the $P(\chi^2)$ calculations.

Stellar ID	Nobs	$\Delta T_{\rm tot}$	Ref
BD+44°493	4	2401	Starkenburg et al. (2014)
HE 1300+0157	6	838	Starkenburg et al. (2014)
BS 16929−005	5	885	Starkenburg et al. (2014)
CS 22877−001	3	4488	Roederer et al. (2014)
CS 22878−027	6	1034	Starkenburg et al. (2014)
CS 29502−092	3	2603	Starkenburg et al. (2014)
CS 22949−037	3	3003	Starkenburg et al. (2014), Roederer et al. (2014)

Notes. Star name, number of additional observations, total time span covered for the star (including NOT observations), and reference.

3.1. Comparison with published radial velocities for the constant stars

Radial-velocity observations for 16 of the programme stars without obvious velocity variations have been published previously, and may help to extend the time span of the data and strengthen our conclusion on their (non-) binary nature. We have searched the literature for velocities of the non-binary stars in our sample, based on moderate- to high-resolution spectra by authors who claim estimated velocity errors of ∼1 km s^{-1} or better. Table B.1 summarises the results of this exercise. We note that these data are typically based on a single observation (or the mean of several closely spaced observations). In each case, the total time span given includes the oldest measurement that we consider reliable.

It is remarkable that no velocity in this comparison sample deviates from our own mean radial velocity by more than can be accounted for by the published errors, especially since the data was obtained with different spectrographs and were reduced and measured independently. As seen from the table, the observed time span for many of our programme stars now covers a decade or more. Clearly, if any of the stars we consider to be single are in fact members of a binary system, they are likely to have extremely long periods (but see discussion below).

An illustrative case is the bright star BD+44°493, which was also observed by Starkenburg et al. (2014). As seen from Tables 2 and B.1, the radial velocities derived by Starkenburg et al. (2014) are in excellent agreement with our derived velocities for both this and other constant stars (all except CS 29502-092 are within the stated 1σ error bars; and CS 29502-092 agrees within 2σ). Radial velocities for BD+44°493 were also reported by Carney et al. (2003) and Ito et al. (2013), whose measured mean velocities of −150.64 km s^{-1} and −150.15 km s^{-1}, respectively, are both in excellent agreement with our result. The Carney et al. data are particularly valuable since they lengthen the three-year time span of our own data by 13 years (1984 to 1997). Together, these four data sets contain 53 measurements spanning a total of 11 368 days (∼31 years) with a standard deviation of 0.63 km s^{-1}. Figure 1 shows all of the radial velocity data for BD+44°493 as a function of time. Clearly, this star is single.

Among the sources of literature data in Table B.1, the only modern series of precise velocities with significant overlap with our programme are those by Starkenburg et al. (2014) and Roederer et al. (2014), whose velocity zero-points, moreover, agree with ours to within ∼100 m s^{-1}. We have therefore included them in our χ^2 calculations, as detailed in Table 3, whenever they could make a significant contribution to our results for the single stars.

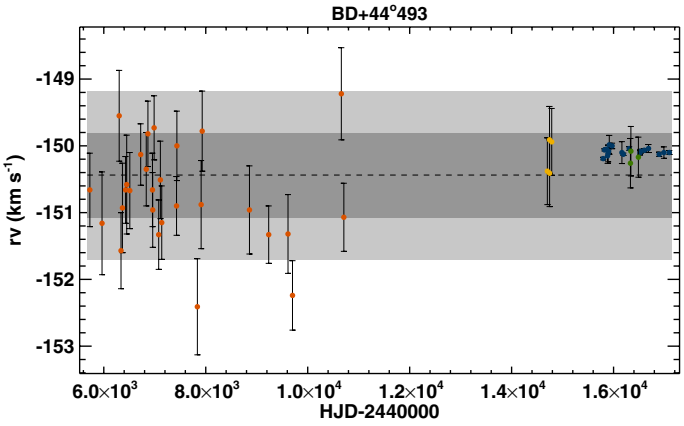

Fig. 1. Radial-velocity history of BD+44°493 vs. time. Blue: this work, red: Carney et al. (2003), yellow: Ito et al. (2013), and green: Starkenburg et al. (2014). Dashed line: global mean radial velocity; grey shaded areas: 1σ and 2σ regions around the global mean.

3.2. Assessment of velocity variability

As discussed above, the data included here were obtained in a systematic manner and are of homogeneous quality, including the selected sources listed in Table 3. In this situation, the χ^2 statistic is the most objective and sensitive indicator of velocity variability as noted, for example by Carney et al. (2003).

In order to assess the binary status of our sample stars, we use the standard χ^2 criterion for velocity variability and compute the probability, $P(\chi^2)$, that the radial velocity is constant, based on the dispersion of the observed velocities vs. their associated internal errors (see Paper I for definitions). A "floor error" term of ∼100 m s^{-1} is added in quadrature to the internal error in order to account for external error sources such as variations in temperature or air pressure, atmospheric dispersion at high airmass, slit positioning, or imperfect guiding.

Observations correlated with the "Delta" template presented special difficulties because of the small number of useful lines in each of the few usable orders in our low-signal spectra. This situation may lead to large stochastic fluctuations in the internal mean error of individual velocities, so that velocities with normal uncertainty, but unusually small or large internal error estimates, completely dominate the overall value of χ^2 or, conversely, are effectively ignored. This is exacerbated in the limiting case of faint and/or extremely metal-poor stars at the limit of what is possible with a 2.5 m telescope when observations obtained under poor conditions cause the correlation with a stellar spectrum to fail altogether.

Alternative attempts to estimate an average overall internal error were found to give results that were effectively biased towards errors that are either too small or too large. However, an

average of the large mean of all internal errors and the smaller error of a mean observation of average weight was found to work reliably, and was adopted in such cases.

Adding the Starkenburg et al. (2014) and Roederer et al. (2014) data listed in Table 3, we then proceeded to calculate $P(\chi^2)$ for potentially single stars. The results, listed in Table 2, demonstrate that the vast majority, 20 of our 24 programme stars, have constant radial velocities over the eight-year period of monitoring (i.e. they appear to be single), while four exhibit obvious radial-velocity variations that are clearly due to orbital motion.

However, limiting cases exist in which low-level variability may be interpreted as due to either motion in a nearly face-on binary orbit as in HE 1523−0901 or to pulsations like those in HE 0017+0055, as is discussed in Sect. 2.1. Since binary orbits that are so very nearly face-on ($i \lesssim 1°$) must be exceedingly rare, finding even one in such a modest sample raises immediate suspicions about its plausibility, such as discussed for the case of HE 1410+0213 in Sect. 3.3 below.

This finding raises another cautionary note concerning the use of Monte Carlo simulations to assess binary frequencies from samples of even accurate, but scattered radial-velocity observations. The limit to the estimated frequency of long-period binaries in the sample may be set by the presence of low-amplitude pulsations rather than merely by observational errors, if orbital motion is considered to be the only possible cause of small velocity variations in the error budget.

3.3. Binaries in our sample of CEMP-no stars

Four stars in our sample exhibited clear orbital motion during the monitoring period: HE 0219−1739, HE 1150−0428, HE 1506−0113, and CS 22957−027. We have determined orbits for three of these systems, combining our radial velocities with earlier, published data. The final orbital parameters for these systems are listed in Table 3, and the radial-velocity curves are shown in Fig. 2, including the literature data and total time spans as noted below. For the Starkenburg et al. (2014) data (red points in Fig. 2), we find an offset of only ∼18 m s^{-1} between our data and theirs based on six constant stars in common. For the data from Preston & Sneden (2001) (green points in Fig. 2), we have applied a correction of ∼1.84 km s^{-1} to achieve consistency with our velocities.

For HE 1506−0113, we were able to combine our ten observations with the seven measurements by Starkenburg et al. (2014), which range from ∼−80 km s^{-1} to −90 km s^{-1}, in good agreement with our own results for this star (see Appendix). Combining them led to a plausible low-amplitude orbit with $P \sim 840$ d and modest eccentricity, although the data were insufficient to determine the orbital parameters with confidence. However, the four constant velocities of ∼−137 km s^{-1} from high-resolution VLT/UVES spectra reported by Norris et al. (2013a), spanning ∼1 month in 2008, did not at all fit this orbit, but could be reconciled with a plausible highly eccentric orbit of $P \sim 950$ d. Nonetheless, the resulting mass function of $f(m) \sim 0.5\ M_\odot$ implied an impossibly high mass for the unseen companion, so this orbit was also rejected.

The large span of the observed velocities led us to re-examine the four archival UVES spectra more closely and to determine fresh radial velocities from them. The results – which are very different – are listed in Table 5 and are plotted as a function of time in Fig. 3. These new velocities are much higher than those reported earlier; they clearly vary over the short observing period ($P(\chi^2) = 0.001$), but delineate a shallow velocity minimum instead of the expected maximum, as is shown in the inset in Fig. 3.

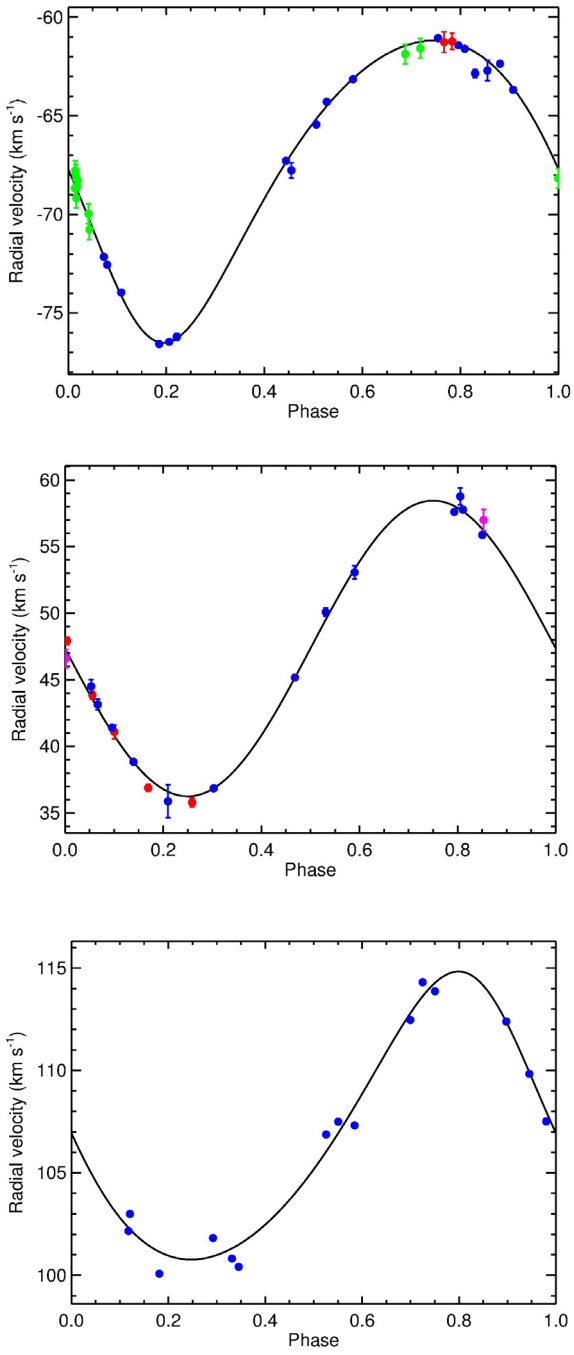

Fig. 2. Orbit solutions for three of the four binaries found among our programme stars. *Top*: CS 22957−027; *middle*: HE 1150−0428; and *bottom*: HE 0219−1739. Blue: this work; red: Starkenburg et al. (2014); green: Preston & Sneden (2001), magenta: Cohen et al. (2013).

Alternative explanations for this recalcitrant behaviour include a triple system or a possible misidentification with a star of similar brightness 15″ SE of HE 1506−0113 itself, but solving this puzzle will require several more years of continued monitoring. In conclusion, and despite persistent effort, we have not been able to compute an orbit for this star, although it is clearly at least a binary.

Table 4 also lists the Roche-lobe radii for the present secondaries in the three binary systems for which we have computed

Table 4. Orbital parameters for three of the binary systems identified in the sample.

Parameter	HE 0219−1739	HE 1150−0428	CS 22957−027
Period (days)	1802.5 ± 5.0	289.7 ± 0.1	1080.0 ± 0.8
T_0 (HJD)	2 455 981.4 ± 1.7	2 455 759.3 ± 0.3	2 455 660.0 ± 1.6
K (km s^{-1})	7.032 ± 0.022	11.102 ± 0.043	7.661 ± 0.039
γ (km s^{-1})	+106.809 ± 0.016	+47.779 ± 0.035	−67.500 ± 0.026
e	0.162 ± 0.004	0.000 ± 0.000	0.193 ± 0.007
ω deg	29.8 ± 1.0	0.0 ± 0.0	155.2 ± 1.6
$a$sin i ($R_\odot$)	247.2 ± 1.0	63.56 ± 0.09	160.5 ± 0.4
$f(m)$ ($M_\odot$)	0.062 ± 0.004	0.041 ± 0.002	0.048 ± 0.003
σ (km s^{-1})	0.867	0.670	0.454
$\Delta T/P$ (total)	1.2	7.7	4.7
$R_{\rm Roche}$ ($R_\odot$, M_1 = 0.8 $M_\odot$, M_2 = 0.4 $M_\odot$)	121	29	73
$R_{\rm Roche}$ ($R_\odot$, M_1 = 0.8 $M_\odot$, M_2 = 1.4 $M_\odot$)	442	131	310

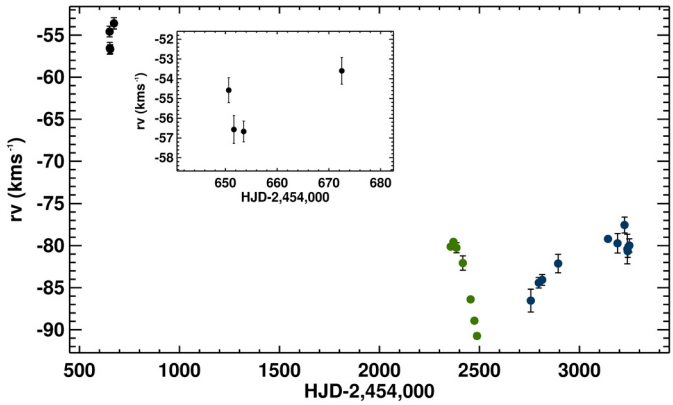

Fig. 3. Radial-velocity data for HE 1506−0113. Blue: this work; green: Starkenburg et al. (2014); and black: re-analysed UVES spectra from Norris et al. (2013a). The inserted box is an enlargement of the RVs obtained from the UVES spectra.

Table 5. Heliocentric radial velocities for HE 1506−0113 from UVES spectra.

HJD	RV	RV$_{\rm err}$
2 454 650.630731	−54.58	0.631
2 454 651.628669	−56.57	0.705
2 454 653.519178	−56.67	0.530
2 454 672.486795	−53.60	0.674

orbits, calculated following the procedure described in Paper I and assuming present primary masses of 0.8 $M_\odot$ and secondary masses of 0.4 and 1.4 $M_\odot$, respectively. These values are the lower and upper limits to the mass of a white dwarf (WD), which would be the likely remnant if the CEMP-no star were polluted by an initially more massive AGB star. As can be seen from Table 4, for the maximum WD mass (1.4 $M_\odot$) all of the systems could have accommodated an AGB star ($R \sim 200\ R_\odot$), while for the lowest WD masses the majority of the Roche-lobes would be too small.

Notes on individual stars

Both Preston & Sneden (2001) and Starkenburg et al. (2014) found significant variations in the velocity of CS 22957−027, but were unable to determine the orbital period with certainty. Our own data allowed us to do so, as kindly confirmed by Dr G. W. Preston (priv. comm.), and the earlier data improved the period determination. Starkenburg et al. (2014) also reported large velocity variations in HE 1150−0428 and HE 1506−0113, but the data were too sparse to determine an orbital period. Our own, more complete data determine the orbit for HE 1150−0428 with certainty (see Fig. 2), while we have not been able to derive an acceptable orbital solution for HE 1506−0113, as discussed above.

HE 1410+0213 presented special difficulties, despite the large number of good observations (Table 2). With $P(\chi^2) < 10^{-4}$, its velocity is certainly variable, and some apparently systematic trends during individual years led us to suspect that it was a nearly face-on spectroscopic binary. Eventually, we were able to derive a plausible circular orbit with a period of ∼330 days and a velocity amplitude of ∼0.28 km s^{-1}. This, however, required an inclination of less than 1°, again highly unlikely in such a small sample of stars. Moreover, a later observation did not fit the putative orbit. We were thus faced with a similar problem to that found for the CEMP-*s* star HE 0017+0055, discussed in Sect. 2.1 and in Paper III.

After much analysis, we conclude that HE 1410+0213 is most probably single, but exhibits low-amplitude pulsations of the kind described by Riebel et al. (2010) for C-rich variables in the LMC. Adding a velocity jitter of 150 m s^{-1} then leads to the value of $P(\chi^2) = 0.196$ given in Table 2.

Mattsson (2015) describes how a combination of a strong stellar wind with such pulsations might enhance the mass loss from such an intrinsically bright EMP giant or AGB star. This could explain why the absolute carbon abundance of HE 1410+0213 places it in the "high-C band" of Spite et al. (2013) discussed below.

Finally, Bonifacio et al. (2009) suggested that CS 29527−015 is a double-lined spectroscopic binary because of asymmetries in the absorption lines detected in their high-resolution, high(er) S/N UVES spectra. We find no evidence for this in our observations of the star, and with $P(\chi^2) = 0.992$ there is also no evidence for any binary motion, but additional high-resolution spectra may be required to settle the issue.

4. Discussion

Our sample of CEMP-no stars comprises 4 binaries and 20 single stars, We thus derive a binary frequency of 17 ± 9%, identical to that found for the *r*-process-enhanced stars in Paper I of this series (18 ± 11%)[3], and to the 16 ± 4% binary frequency

[3] We have corrected the error on this frequency reported in Paper I, which was incorrectly stated to be ±6%.

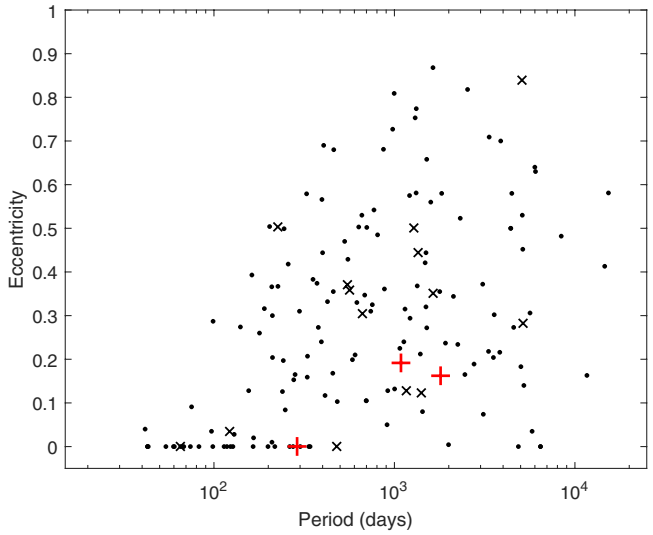

Fig. 4. Period–eccentricity distribution for the binary systems in our sample (red plus signs) compared to literature data (black dots: Population I cluster giants, Mermilliod et al. 2007; Mathieu et al. 1990 and black crosses: Population I giants, Carney et al. 2003).

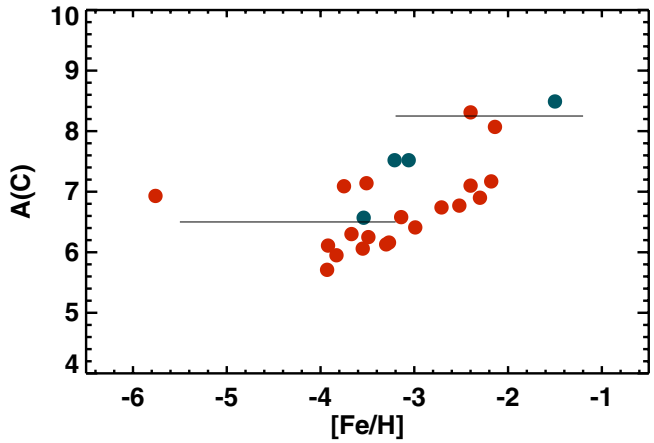

Fig. 5. Absolute carbon abundances, $A(\mathrm{C}) = \log \epsilon(\mathrm{C})$, of our programme stars as a function of metallicity, [Fe/H]. Blue dots represent recognised binaries in our sample; red dots represent non-binaries. The high-C and low-C bands of Spite et al. (2013) are indicated by the horizontal lines.

found by Carney et al. (2003) in their study of 91 metal-poor ([Fe/H] ≤ -1.4) field red giants.

4.1. Binary parameters and their implications

The four binary systems in our sample exhibit a similar combination of periods and eccentricities to those for metal-poor field red giants and dwarfs that Carney et al. (2003) found (see their Fig. 5), for Population I cluster giants that Mermilliod et al. (2007) found, and for the *r*-process-enhanced VMP and EMP stars that we found (see Paper I). Figure 4 shows the period–eccentricity distribution for our binary stars (red plus signs) compared to the literature data from Mermilliod et al. (2007), Mathieu et al. (1990) (black dots), and Carney et al. (2003) (black crosses). The properties of our binary stars are thus completely indistinguishable from those of chemically normal population I and II giants, with HE 1150−0428 defining a cutoff period for circular orbits of old giant stars of $\gtrsim$300 days, presumably due to the long time available for tidal circularisation.

This simple observational finding indicates that membership of a binary system has played no causal role in generating the dramatic carbon excess of the CEMP-no stars and rules out the local mass-transfer scenario for its origin. Instead, the excess carbon must have been produced elsewhere and implanted across interstellar distances into the natal cloud of the star we observe today, a process that is not included in standard models of the early chemical evolution of galaxy haloes.

4.2. Carbon bands

Spite et al. (2013) first suggested the existence of two bands in the absolute carbon abundances of CEMP stars: a high-C band at $A(\mathrm{C}) \sim 8.25$ and a low-C band at $A(\mathrm{C}) \sim 6.5$. Stars with carbon abundances on the lower band are more metal poor ([Fe/H] $\lesssim -3.0$) and are mostly of the CEMP-no variety, while those on the higher band are relatively more metal rich ([Fe/H] $\gtrsim -3.0$) and are primarily CEMP-*s* stars. They suggested that stars on the high-C band are members of binary systems that have been polluted by a companion AGB star, i.e. their carbon enhancement is extrinsic, whereas the stars on the low-C band were born from an ISM that had already been polluted by a presumably high-mass progenitor, i.e. the carbon enhancement is thus intrinsic to the star.

The existence of these two bands for CEMP stars has been confirmed with larger samples by Bonifacio et al. (2015) and Hansen et al. (2015a). Both of these samples find CEMP-no stars with carbon abundances placing them on the high-C band, but neither of these papers had sufficient information available to address the binary nature of their stars, and thereby more fully test the hypothesis for the astrophysical origin of the bands. Figure 5 shows the absolute carbon abundances of the stars in our sample as a function of metalicity; blue dots represent the detected binary stars and red dots represent the single stars.

As can be seen from inspection of Fig. 5, three of our CEMP-no stars (HE 0219−1739, HE 1133−0555, and HE 1410+0213) have carbon abundances corresponding to the high-C band. HE 0219−1739 is a binary with ample space to accommodate a companion at the AGB stage in its Roche-lobe for the assumed minimum and maximum masses (0.4 $M_\odot$ and 1.4 $M_\odot$) of the putative white dwarf remnant (Table 3). HE 1410+0213 and HE 1133−0555 are both most likely single stars, but HE 1410+0213 is pulsating (see discussion above), which could enhance any mass loss by a strong stellar wind.

Two of the more metal-poor binary stars have carbon abundances that lie in the transition area between the two bands, around [Fe/H] ~ -3.0, where both CEMP-no and CEMP-*s* stars can be found. These two stars are HE 1150−0428 and CS 22957−027 (see Fig. 2), the former having a circular orbit with a period of $P = 290$ days and the latter having a slightly eccentric orbit with a period of $P = 1080$ days. Only one of the stars with an absolute carbon abundance clearly on the low band is found to be in a binary system, HE 1506−0113. This star also exhibits high Na and Mg abundance ratios ([Na/Fe] = +1.65 and [Mg/Fe] = +0.89; Yong et al. 2013), signatures that are also found for many other CEMP-no stars (Norris et al. 2013b; Hansen et al. 2015a). It is worth noting that HE 1150−0428 also exhibits a high Na abundance [Na/Fe] = +1.31, but normal Mg abundance [Mg/Fe] = +0.36 (Cohen et al. 2013). For CS 22957−027, Cohen et al. (2013) report a high Na abundance ratio ([Na/Fe] = +0.80), but a low Mg ratio

([Mg/Fe] = +0.11), while Aoki et al. (2002c) obtain a higher Mg ratio ([Mg/Fe] = +0.69).

It is clearly highly desirable to obtain further information on the possible binary nature of the other six CEMP-no stars with carbon abundances on the high-C band, found in previous work (Bonifacio et al. 2015; Hansen et al. 2015a), and expand the sample of such stars. Should the majority turn out to be members of binary systems (rather unlikely in view of our present results), and in particular if there are signs that mass transfer has occurred, this would lend support to the existence of AGB stars that produce little if any *s*-process elements. A new nucleosynthesis process might then need to be invoked, or our understanding of the operation of the *s*-process at low metallicity must be improved. If these stars are also found to be single, another, distant production site must be invoked.

4.3. Evidence that CEMP-no stars are indeed second-generation stars

Our primary result from this paper confirms (with much-improved statistics) that mass transfer from a binary companion is not a necessary condition to account for the distinctive elemental-abundance patterns of CEMP-no stars. This is already strong evidence that they may indeed be bona fide second-generation stars, formed from an ISM polluted by a previous (possibly first-generation) population of stars. However, this is not the only evidence for this association. Here we briefly summarise the present observational constraints on this hypothesis.

- *The increased frequency of CEMP stars at low metallicity*: It has been recognised for over a decade that the relative numbers of CEMP stars (compared to C-normal stars) increases dramatically as [Fe/H] declines from [Fe/H] = −2.0 to the most Fe-poor star known (SMSS J0313-6708, with [Fe/H] $\lesssim$ −7.8; Keller et al. 2014; Bessell et al. 2015). Recent large samples of VMP and EMP stars from SDSS/SEGUE (Sloan Digitial Sky Survey / Sloan Extension for Galactic Understanding and Exploration, Lee et al. 2013), have reinforced this result based on the thousands of CEMP stars found in this survey. It has also been shown that at the lowest metalicities the CEMP-no stars are the dominant subclass of CEMP stars (Aoki et al. 2007; Norris et al. 2013b). When limited to the sample of recognised or likely CEMP-no stars, the derived frequencies increase by 5–10% relative to CEMP stars when considered as a single class (Placco et al. 2014a). It has also been argued by Bromm & Loeb (2003) and Frebel et al. (2007a) that high C and O abundances facilitate low-mass star formation in the early Universe, resulting in the birth of long-lived C-enhanced stars.

- *The dominance of CEMP-no stars among C-enhanced stars at the lowest metallicity*: Aoki et al. (2007) found a clear difference in the metallicity distributions of CEMP-no and CEMP-*s* stars: the CEMP-no stars in their sample primarily occupy the lowest metallicity range (and are the only C-enhanced stars found below [Fe/H] = −3.3 in their sample). At even lower metallicities, seven of the eight stars known with [Fe/H] < −4.5: SMSS J0313−6708 ([Fe/H] $\leq$ −7.8, Keller et al. 2014; Bessell et al. 2015); HE 1327−2326 ([Fe/H] = −5.7, Frebel et al. 2006; Aoki et al. 2006), HE 0107−5240 ([Fe/H] = −5.4, Christlieb et al. 2004), SDSS J1313−0019 ([Fe/H] = −5.0, Allende Prieto et al. 2015; Frebel et al. 2015), HE 0557−4840 ([Fe/H] = −4.8, Norris et al. 2007), SDSS J1742+2531 ([Fe/H] = −4.8, Bonifacio et al. 2015), SDSS J1029+1729 ([Fe/H] = −4.7, Caffau et al. 2011), and HE 0233−0343 ([Fe/H] = −4.7, Hansen et al. 2014) are CEMP-no stars. The star SDSS J035+0641 may be added to this list in the near future (Bonifacio et al. 2015 report [Ca/H] = −5.0). The lone exception is SDSS J1029+1729, for which Caffau et al. (2011) report [C/Fe] $\leq$ +0.9, but higher S/N data is required in order to be certain of its status.

- *The sequence of the CEMP-no and EMP r-II stars*: As noted above, the composition of the mostly single CEMP-no stars is dominated by carbon, while the iron-peak elements are very weak ([Fe/H] < −3.0 to < −3.5). The strongly *r*-process-element enhanced (*r*-II) stars appear in a relatively narrow metallicity range near [Fe/H] = −3.0 and are mostly single, while the less-enhanced (i.e. more iron-rich) *r*-I stars have higher metallicities. However, the extreme *r*-II stars CS 31082−001 and HE 1523-0901, which are not C-rich, have absolute age determinations of ∼13–14 Gyr from direct radioactive U/Th chronology (Hill et al. 2002; Frebel et al. 2007b), so one would reasonably expect the CEMP-no stars to be even older, at least in a chemical sense.

- *The bimodal distribution of A(C) for CEMP stars*: As discussed above, the recent recognition that the absolute carbon abundance of CEMP stars is apparently bimodal clearly indicates that a source of carbon production other than that associated with AGB stars is required in the early Universe.

- *The Li abundances of CEMP-no stars*: As discussed by Hansen et al. (2014) and references therein, the observed abundances of lithium for CEMP-no stars are all below the Spite Li plateau. While many of these stars may have had their Li depleted by internal mixing during giant branch evolution, this does not apply to all cases (HE 1327−2326, for example, is a warm subgiant with very low Li; several other such stars are listed in Masseron et al. 2012). This provides support for the suggestion by Piau et al. (2006) that Li astration by the progenitors associated with the production of carbon in the CEMP-no stars, followed by mixing with primordial gas, may well be involved.

- *The observed Be and B abundance limits for BD+44°493*: The elements Be and B are thought to form in the early Universe exclusively by spallation reactions involving high-energy cosmic rays (Prantzos 2012), which implies that the abundances of these elements in CEMP-no stars should be uniformly low if they are indeed second-generation stars (due to the lack of a significant background cosmic-ray flux at these early times). Placco et al. (2014b) indeed reported very low upper limits for the abundances of Be and B in BD+44°493 ($\log\epsilon$ (Be) < −2.3 and $\log\epsilon$ (B) < −0.7). A low upper limit for Be ($\log\epsilon$ (Be) < −1.8) was also previously found by Ito et al. (2013) for this star. Although future observations (from the ground for Be, from space for B) are required for additional CEMP-no stars, the results for BD+44°493 are already compelling.

- *The association of CEMP-no stars with the outer-halo population of the Galaxy*: Carollo et al. (2012) confirmed the early suggestion by Frebel et al. (2006; see also Beers et al., in prep.) that the fraction of CEMP stars increases with

distance from the Galactic plane. The Carollo et al. study also showed a significant contrast in the frequency of CEMP stars between the inner- and outer-halo components of the Milky Way, with the outer halo having roughly twice the fraction of CEMP stars as the inner halo. They interpreted this as an indication that the progenitor population(s) of the outer halo likely had additional astrophysical sources of carbon production, beyond the AGB sources that may dominate for inner-halo stars.
Subsequently, Carollo et al. (2014) offered evidence that the CEMP-*s* stars are preferentially associated with the inner-halo population, while the CEMP-no stars appear more strongly associated with the outer-halo population. As pointed out by Carollo et al. (2014), recent hierarchical galaxy-formation simulations suggest that the inner-halo population of the Milky Way arose from the assembly of relatively more massive sub-galactic fragments (capable of supporting extended star formation, hence reaching higher metallicities), while the outer-halo population comprises stars formed in relatively less massive fragments (which experienced short or truncated star-formation histories, and hence produced stars of lower metallicity). This and other lines of evidence (e.g. the likely flatter IMF associated with star formation in the early Universe; Tumlinson 2007) suggest that the dominant progenitors of CEMP stars in the two halo components were different: massive stars for the outer halo and intermediate-mass stars in the case of the inner halo.

– *The discovery of damped Ly-alpha systems with enhanced carbon*: Cooke et al. (2011, 2012) have reported on recently discovered high-redshift carbon-enhanced damped Ly-alpha systems that exhibit elemental-abundance patterns which resemble those expected from massive, carbon-producing first stars, and speculated that these progenitors are the same as those responsible for the abundance patterns associated with CEMP-no stars in the Galaxy. To our knowledge, this is one of the first cases of evidence, if not the first, for a direct link between the observed abundances in cosmologically distant objects with local extremely metal-poor stars. It also underscores our main conclusion that the excess carbon was not provided by a binary companion, but was produced elsewhere and transported across interstellar distances through the early ISM.

5. Conclusions and outlook

We have systematically monitored the radial velocities for a sample of 24 CEMP-no stars for time spans of up to eight years, and confidently identify a total of four binary systems. We have identified a number of other CEMP-no stars in the literature, not included in our own programme, which similarly exhibit no signs of binarity. These include the hyper metal-poor star HE 0107−5240 with RV_{mean} = 44.5 km s^{-1} and σ = 0.3 km s^{-1} (31 measurements from 2001 to 2006; N. Christlieb, priv. comm.), the ultra metal-poor star HE 0557−4840 with RV_{mean} = 211.7 km s^{-1} and σ = 0.2 km s^{-1} over 2193 days (Norris et al. 2007, 2012), and the EMP star CD −24°17504 with RV_{mean} = 136.6 km s^{-1} and σ = 0.7 km s^{-1} over 4739 days (Norris et al. 2001; Aoki et al. 2009; Jacobson et al. 2015). All of these stars have carbon abundances on the low-C band, whereas the majority of our detected binary stars have carbon abundances either in the transition area between the two bands-an area populated by both CEMP-no and CEMP-*s* stars-or on the high-C band.

There is clearly a need for additional RV monitoring observations of CEMP-no (and CEMP-*s*) stars (see Paper III of this series), and detailed abundance analyses of these stars in order to identify more examples of high/low carbon-band associations, and to better understand the astrophysical implications. The ongoing survey by Placco et al. to detect bright CEMP targets from among RAVE stars with [Fe/H] < −2 (Kordopatis et al. 2013) will be an ideal source of candidates for radial-velocity monitoring, once they can be confirmed as CEMP-no or CEMP-*s* stars. In addition, stars emerging from surveys such as SkyMapper (Keller et al. 2007, 2014; Jacobson et al. 2015), the TOPoS survey of SDSS/SEGUE turnoff stars (Caffau et al. 2013; Bonifacio et al. 2015), and LAMOST (Deng et al. 2012; Li et al. 2015) will help to further populate and confirm the existence of the two carbon bands.

We conclude that compelling evidence now exists that the CEMP-no stars are among the first low-mass stars to form in the early Universe, and as such they contain the chemical imprints of the very first stars in their natal clouds in the early ISM. The prime candidates for the production of large amounts of carbon in the early Universe are faint supernovae with mixing and fallback (Umeda & Nomoto 2003; Nomoto et al. 2013) and massive, rapidly rotating metal-free stars, the so-called spinstars (Meynet et al. 2006; Hirschi 2007; Maeder et al. 2015).

Thus far, no clear distinction between the abundance patterns of these two scenarios has been found, either in the models or in the derived abundances of the CEMP-no stars. The observed large overabundances of carbon and nitrogen are reproduced well by both models. The spinstar model can also explain other signatures found in CEMP-no stars, such as low $^{12}C/^{13}C$ isotopic ratios, and high Na, Mg, Al, and Sr abundances (Maeder et al. 2015), while Tominaga et al. (2014) was able to fit the abundance patterns of 12 CEMP-no stars, from C to Zn, with yields from mixing and fallback SNe models.

However, at present none of the suggested progenitors can explain the full range of elements for which abundances are derived for CEMP-no stars: the light-elements, the α-elements, the iron-peak elements, and the neutron-capture elements. Hence, as suggested by Takahashi et al. (2014), the observed abundance patterns of CEMP-no stars (perhaps in particular those in the transition area between the low-C and high-C bands) could arise from a combination of the two suggested progenitors, or another primordial source that has yet to be identified. Detailed abundance analyses of larger samples of CEMP-no stars will help to settle this question.

Acknowledgements. We thank several NOT staff members and students for obtaining most of the FIES observations for us in service mode during this large project. We thank Piercarlo Bonifacio and Monique Spite for sharing their previously obtained spectrum of CS 29527-015 and for obtaining a new upper limit on the [Ba/Fe] ratio for this star, George Preston for very kindly sharing his own observations of CS 22957−027, and Norbert Christlieb for sharing his RV data for HE 0107−5240 with us. We also thank Heather Jacobsen for advice on the best available historical RV data for CD-24°17504, and David Yong for helping to clarify some of the mystery regarding HE 1506−0113. Furthermore, we express our cordial thanks to the referee for an incisive and helpful report, which led to substantial improvements in the paper. T.T.H. was supported during this work by Sonderforschungsbereich SFB 881 "The Milky Way System" (subproject A4) of the German Research Foundation (DFG). J.A. and B.N. gratefully acknowledge financial support from the Danish Natural Science Research Council and the Carlsberg Foundation, and T.C.B., V.M.P., and J.Y. acknowledge partial support for this work from grants PHY 08-22648; Physics Frontier Center/Joint Institute or Nuclear Astrophysics (JINA), and PHY 14-30152; Physics Frontier Center/JINA Center for the Evolution of the Elements (JINA-CEE), awarded by the US National Science Foundation. This paper is based primarily on observations made with the Nordic Optical Telescope, operated by the Nordic Optical Telescope Scientific Association at the Observatorio del Roque de los

Muchachos, La Palma, Spain, of the Instituto de Astrofisica de Canarias. It is also based on observations obtained at the Southern Astrophysical Research (SOAR) telescope, which is a joint project of the Ministério da Ciência, Tecnologia, e Inovação (MCTI) da República Federativa do Brasil, the US National Optical Astronomy Observatory (NOAO), the University of North Carolina at Chapel Hill (UNC), and Michigan State University (MSU).

References

Abate, C., Pols, O. R., Izzard, R. G., et al. 2013, A&A, 552, A26
Abate, C., Pols, O. R., Stancliffe, et al. 2015, A&A, 581, A62
Allende Prieto, C., Fernández-Alvar, E., Aguado, D. S., et al. 2015, A&A, 579, A98
Aoki, W., Norris, J. E., Ryan, S. G., Beers, T. C., & Ando, H. 2002a, ApJ, 567, 1166
Aoki, W., Ando, H., Honda, S., et al., 2002b, PASJ, 54, 427
Aoki, W., Norris, J. E., Ryan, S. G., Beers, T. C., & Ando, H. 2002c, ApJ, 576, L141
Aoki, W., Norris, J. E., Ryan, S. G., et al. 2004, ApJ, 608, 971
Aoki, W., Frebel, A., Christlieb, N., et al. 2006, ApJ, 639, 897
Aoki, W., Beers, T. C., Christlieb, N., et al. 2007, ApJ, 655, 492
Aoki, W., Barklem, P. S., Beers, T. C., et al. 2009, ApJ, 698, 1803
Aoki, W., Beers, T. C., Lee, Y. S., et al. 2013, AJ, 145, 13
Asplund, M., Grevesse, N., Sauval, A. J., & Scott, P. 2009, ARA&A, 47, 481
Barklem, P. S., Christlieb, N., Beers, T. C., et al. 2005, A&A, 439, 129
Beers, T. C., & Christlieb N. 2005, ARA&A, 43, 531
Beers, T. C., Preston, G. W., & Shectman, S. A. 1985, AJ, 90, 2089
Beers, T. C., Preston, G. W., & Shectman, S. A. 1992, AJ, 103, 1987
Beers, T. C., Flynn, C., Rossi, S., et al. 2007, ApJS, 168, 128
Beers, T. C., Norris, J. E., Placco, V. M., et al. 2014, ApJ, 794, 58
Bessell, M. S., Collet, R., Keller, S. C., et al. 2015, ApJ, 806, L16
Bonifacio, P., Spite, M., Cayrel, R., et al. 2009, A&A, 501, 519
Bonifacio, P., Caffau, E., Spite, M., et al. 2015, A&A, 579, A28
Bromm, V., & Loeb, A. 2003, Nature, 425, 812
Caffau, E., Bonifacio, P., Francois, P., et al. 2011, Nature, 477, 67
Caffau, E., Bonifacio, P., Sbordone, L., et al. 2013, A&A, 560, A71
Carney, B. W., & Latham, D. W. 1986, AJ, 92, 60
Carney, B. W., Latham, D. W., Stefanik, R. P., Laird, J. B., & Morse, J. A. 2003, AJ, 125, 293
Carollo, D., Beers, T. C., Bovy, J., et al. 2012, ApJ, 744, 195
Carollo, D., Freeman, K., Beers, T. C., et al. 2014, ApJ, 788, 180
Cayrel, R., Depagne, E., Spite, M., et al. 2004, A&A, 416, 1117
Christlieb, N., Gustafsson, B., Korn, A. J., et al. 2004, ApJ, 603, 708
Christlieb, N., Schörck, T., Frebel, A., et al. 2008, A&A, 484, 721
Cohen, J. G., Christlieb, N., McWilliam, A., et al. 2008, ApJ, 672, 320
Cohen, J. G., Christlieb, N., Thompson, I., et al. 2013, ApJ, 778, 56
Cooke, R., Pettini, M., Steidel, C. C., Rudie, G. C., & Jorgenson, R. A. 2011, MNRAS, 412, 1047
Cooke, R., Pettini, M., & Murphy, M. T. 2012, MNRAS, 425, 347
Deng, L. C., Newberg, H. J., Liu, C., et al. 2012, RA&A, 12, 735
Depagne, E., Hill, V., Spite, M., et al. 2002, A&A, 390, 187
Duquennoy, A., & Mayor, M. 1991, A&A, 248, 485
Frebel, A., & Norris, J. E. 2015, ARA&A, 53, 631
Frebel, A., Christlieb, N., Norris, J. E., Aoki, W., & Asplund, M. 2006, ApJ, 638, L17
Frebel, A., Johnson, J. L., & Bromm, V. 2007a, MNRAS, 380, L40
Frebel, A., Christlieb, N., Norris, J. E., et al. 2007b, ApJ, 660, L117
Frebel, A., Collet, R., Eriksson, K., Christlieb, N., & Aoki, W. 2008, ApJ, 684, 588
Frebel, A., Chiti, A., Ji, A. P., Jacobson, H. R., & Placco, V. M. 2015, ApJ, 810, L27
Giridhar, S., Lambert, D. L., Gonzalez, G., & Pandey, G. 2001, PASP, 113, 519
Hansen, T., Andersen, J., Nordström, B., Buchhave, L., & Beers, T. C. 2011, ApJ, 743, L1
Hansen, T., Hansen, C. J., Christlieb, N., et al. 2014, ApJ, 787, 162
Hansen, T., Hansen, C. J., Christlieb, N., et al. 2015a, ApJ, 807, 173
Hansen, T. T, Andersen, J., Nordström, B., et al. 2015b, A&A, 583, A49 (Paper I)
Hansen, T. T., Andersen, J., Nordström, B., et al. 2015c, A&A, submitted (Paper III)
Henden, A. A., Levine, S., Terrell, D., & Welch, D. L. 2015, AAS Meet. Abstr., 225, 336.16
Hill, V., Plez, B., Cayrel, R., et al. 2002, A&A, 387, 560
Hirschi, R. 2007, A&A, 461, 571
Honda, S., Aoki, W., Ando, H., et al. 2004, ApJS, 152, 113
Ito, H., Aoki, W., Beers, T. C., Tominaga, N., Honda, S., & Carollo, D. 2013, ApJ, 773, 33
Ivezic, Z., Beers, T. C., & Juric, M. 2012, ARA&A, 50, 251
Izzard, R. G., Glebbeek, Stancliffe, R. J., & Pols, O. R. 2009, A&A, 508, 1359
Jacobson, H., & Frebel, A. 2015, ApJ, 808, 53
Jacobson, H., Keller, S., Frebel, A., et al. 2015, ApJ, 807, 171
Jorissen, A., Hansen, T., Van Eck, S., et al. 2016, A&A, 586, A159
Keller, S. G., Schmidt, B. P., Bessell, M. S., et al. 2007, PASA, 24, 1
Keller, S. C., Bessell, M. S., Frebel, A., et al. 2014, Nature, 506, 463
Kordopatis, G., Gilmore, G., Steinmetz, M., et al. 2013, AJ, 146, 134
Kupka, F., Piskunov, N., Ryabchikova, T. A., Stempels, H. C., & Weiss, W. W. 1999, A&AS, 138, 119
Lai, D. K., Bolte, M., Johnson, J. A., & Lucatello, S. 2004, AJ, 128, 2402
Lai, D K., Bolte, M., Johnson, J. A., et al. 2008, ApJ, 681, 1524
Lee, Y. S., Beers, T. C., Masseron, T., et al. 2013, AJ, 146, 132
Li, H., Zhao, G., Christlieb, N., et al. 2015, ApJ, 798, 110
Lucatello, S., Tsangarides, S., Beers, T. C., et al. 2005, ApJ, 625, 825
Maeder, A., Meynet, G., & Chiappini, C. 2015, A&A, 576, A56
Masseron, T., Johnson, J., Lucatello, S., et al. 2012, ApJ, 751, 14
Mathieu, R. D., Latham, D. W., & Griffin, R. F. 1990, AJ, 100, 1899
Mattsson, L. 2015, MNRAS, submitted [arXiv:1505.04758]
Mcwilliam, A., Preston, G. W., Sneden, C., & Shectman, S. 1995, AJ, 109, 2736
Mermilliod, J.-C., Andersen, J., Latham, D. W., & Mayor, M. 2007, A&A, 473, 829
Meynet, G., Ekström, S., & Maeder, A. 2006, A&A, 447, 623
Nomoto, K., Kobayashi, C., & Tominaga, N. 2013, ARA&A, 51, 457
Nordström, B., Andersen, J., & Andersen, M. I. 1997, A&A, 322, 460
Norris, J. E., Ryan, S. G., & Beers, T. C. 1996, ApJS, 107, 391
Norris, J. E., Ryan, S. G., & Beers, T. C. 1999, ApJS, 123, 639
Norris, J. E., Ryan, S. G., & Beers, T. C. 2001, ApJ, 561, 1034
Norris, J. E., Christlieb, N., Korn, A. J., et al. 2007, ApJ, 670, 774
Norris, J. E., Christlieb, N., Bessell, M. S., et al. 2012, ApJ, 753, 150
Norris, J. E., Bessell, M. S., Yong, D., et al. 2013a, ApJ, 762, 25
Norris, J. E., Yong, D., Bessell, M. S., et al. 2013b, ApJ, 762, 28
Piau, L., Beers, T. C., Balsara, D. S., et al. 2006, ApJ, 653, 300
Placco, V. M., Frebel, A., Beers, T. C., et al. 2014a, ApJ, 781, 40
Placco, V. M., Beers, T. C., Roederer, I. U., et al. 2014b, ApJ, 790, 34
Prantzos, N. 2012, A&A, 542, 67
Preston, G. W., & Sneden, C. 2001, AJ, 122, 1545
Preston, G. W., Shectman, S. A., & Beers, T. C. 1991, ApJS, 76, 1001
Riebel, D., Meixner, M., Fraser, O. et al., ApJ, 723, 1195
Roederer I. U., Preston, G. W., Thompson, I. B. 2014, AJ, 147, 136
Ruchti, G. R., Fulbright, J. P., Wyse, R. F. G., et al. 2011, ApJ, 737, 9
Ryan, S. G., Aoki, W., Norris, J. E., & Beers, T. C. 2005, ApJ, 635, 349
Sakari, C. M., Shetrone, M., Venn, K., McWilliam, A., & Dotter, A. 2013, MNRAS, 343, 358
Spite, M., Caffau, E., Bonifacio, P., et al. 2013, A&A, 552, A107
Starkenburg, E., Shetrone, M. D., McConnachie, A. W., & Venn, K. A. 2014, MNRAS, 411, 1217
Takahashi, K., Umeda, H., & Yoshida, T. 2014, ApJ, 794, 40
Tominaga, N., Iwamoto, N., & Nomoto, K. 2014, ApJ, 785, 98
Tsangarides, S. A., Ryan, S. G., & Beers, T. C. 2003, in ASP Conf. Ser. 304, eds. C. Charbonnel, D. Schaerer, & G. Meynet, 133
Tumlinson, J. 2007, ApJ, 665, 1361
Umeda, H., & Nomoto, K. 2003, Nature, 422, 871
Yong, D., Norris, J. E., Bessell, M. S., et al. 2013, ApJ, 762, 26

Appendix A: Heliocentric radial velocities measured for the programme stars

Table A.1. HE 0020−1741.

HJD	RV km s^{-1}	RV$_{err}$ km s^{-1}
2 456 191.553850	92.761	0.061
2 456 277.325704	92.678	0.085
2 456 530.727938	93.249	0.068
2 456 545.641765	93.144	0.053
2 456 603.431706	92.993	0.073
2 456 893.629396	93.214	0.062
2 456 986.461205	93.201	0.076
2 457 225.690882	92.920	0.114
2 457 257.705129	93.192	0.093

Table A.2. CS 29527−015.

HJD	RV km s^{-1}	RV$_{err}$ km s^{-1}
2 456 193.657074	47.032	1.730
2 456 214.489204	46.880	0.500
2 456 531.626981	47.136	0.083
2 456 603.479383	46.536	1.830
2 456 895.609724	47.777	1.405
2 457 257.602490	47.371	1.314

Table A.3. CS 22166−016.

HJD	RV km s^{-1}	RV$_{err}$ km s^{-1}
2 456 191.570891	−210.289	0.220
2 456 300.388000	−210.344	0.242
2 456 531.654302	−210.477	0.161
2 456 579.603014	−210.404	0.183
24 56 652.456871	−209.670	0.903
2 456 895.638248	−210.397	0.036
2 456 956.601783	−212.384	1.018
2 457 225.706367	−210.071	0.269

Table A.4. HE 0219−1739.

HJD	RV km s^{-1}	RV$_{err}$ km s^{-1}
2 454 396.611647	102.993	0.064
2 454 705.669847	101.817	0.056
2 455 126.606616	106.873	0.057
2 455 171.488102	107.500	0.056
2 455 232.347099	107.317	0.051
2 455 439.645440	112.468	0.041
2 455 485.610217	114.309	0.046
2 455 531.495382	113.868	0.063
2 455 796.705307	112.387	0.037
2 455 882.508124	109.832	0.065
2 455 945.426690	107.516	0.151
2 456 193.705723	102.161	0.052
2 456 308.451562	100.074	0.087
2 456 578.607672	100.814	0.052
2 456 603.608463	100.413	0.082

Table A.5. BD+44°493.

HJD	RV km s^{-1}	RV$_{err}$ km s^{-1}
2 455 796.731150	−150.191	0.019
2 455 821.602481	−150.061	0.016
2 455 859.544117	−150.050	0.017
2 455 882.390816	−150.150	0.113
2 455 892.414452	−150.114	0.125
2 455 903.488584	−150.080	0.032
2 455 915.503192	−149.985	0.141
2 455 971.385310	−150.001	0.041
2 456 163.698695	−150.101	0.164
2 456 191.605915	−150.126	0.018
2 456 307.434407	−150.041	0.028
2 456 518.689701	−150.104	0.031
2 456 528.699713	−150.081	0.028
2 456 603.638647	−150.066	0.025
2 456 685.418052	−150.040	0.060
2 456 893.598206	−150.127	0.032
2 456 987.491755	−150.101	0.086
2 457 094.349390	−150.100	0.029

Table A.6. HE 0405−0526.

HJD	RV km s^{-1}	RV$_{err}$ km s^{-1}
2 456 190.761992	165.656	0.014
2 456 209.746333	165.593	0.057
2 456 213.772353	165.684	0.032
2 456 241.709356	165.674	0.057
2 456 340.434828	165.568	0.110
2 456 528.683688	165.668	0.029
2 456 603.556421	165.639	0.017
2 456 685.438636	165.676	0.019
2 456 686.360900	165.708	0.021
2 456 726.353768	165.667	0.071
2 456 986.480120	165.662	0.024
2 457 018.579283	165.700	0.034
2 457 094.366572	165.641	0.023

Table A.7. HE 1012−1540.

HJD	RV km s^{-1}	RV$_{err}$ km s^{-1}
2 456 340.537113	225.915	1.827
2 456 426.386869	225.897	0.373
2 456 458.405646	225.707	1.198
2 456 752.448580	226.178	0.180
2 456 796.400824	226.154	0.296
2 456 987.772426	226.366	0.536
2 457 076.586146	226.040	2.439
2 457 142.415352	226.161	0.349

Table A.8. HE 1133−0555.

HJD	RV km s^{-1}	RV$_{err}$ km s^{-1}
2 454 951.480644	270.638	0.226
2 455 207.661330	270.604	0.173
2 455 738.452327	271.020	0.561
2 456 005.578838	270.387	0.450
2 456 033.538287	269.999	0.599
2 456 307.743507	270.534	0.393
2 456 426.426846	270.804	0.159
2 456 796.484997	271.130	0.328
2 457 168.502711	270.575	0.537

Table A.9. HE 1150−0428.

HJD	RV km s^{-1}	RV$_{err}$ km s^{-1}
2 454 254.469526	59.198	0.631
2 454 464.774604	50.506	0.305
2 454 481.794575	53.500	0.493
2 454 909.540207	43.574	0.403
2 454 930.649908	39.265	0.104
2 455 207.697467	41.831	0.220
2 455 704.477220	58.205	0.053
2 456 005.672746	56.305	0.094
2 456 064.445022	44.939	0.506
2 456 278.762138	58.039	0.192
2 456 399.466063	36.305	1.247
2 456 426.466103	37.280	0.053
2 456 474.416329	45.598	0.078

Table A.10. HE 1201−1512.

HJD	RV km s^{-1}	RV$_{err}$ km s^{-1}
2 456 722.550471	242.676	2.665
2 456 756.503043	238.280	2.525
2 456 814.436159	238.593	1.086
2 457 110.570965	238.337	...
2 457 142.522877	239.365	0.705

Table A.11. HE 1300+0157.

HJD	RV km s^{-1}	RV$_{err}$ km s^{-1}
2 456 756.542595	75.397	0.531
2 456 796.569354	74.182	0.418
2 456 840.398240	75.141	0.321
2 457 142.604191	73.800	0.284
2 457 168.543909	74.159	0.146

Table A.12. BS 16929−005.

HJD	RV km s^{-1}	RV$_{err}$ km s^{-1}
2 456 340.583325	−50.188	2.672
2 456 426.503527	−51.478	0.973
2 456 652.666926	−50.625	1.020
2 456 722.615544	−50.970	1.810
2 456 756.432118	−49.880	1.415
2 457 096.737115	−50.575	0.166
2 457 225.402088	−51.430	0.814

Table A.13. HE 1300−0641.

HJD	RV km s^{-1}	RV$_{err}$ km s^{-1}
2 456 756.628997	68.926	0.893
2 457 142.577242	68.765	0.405

Table A.14. HE 1302−0954.

HJD	RV km s^{-1}	RV$_{err}$ km s^{-1}
2 456 756.590880	32.494	0.268
2 457 111.063422	32.549	0.229
2 457 142.552710	32.570	0.124

Table A.15. CS 22877−001.

HJD	RV km s^{-1}	RV$_{err}$ km s^{-1}
2 454 219.526768	166.288	0.071
2 454 254.500103	166.360	0.075
2 454 909.559431	166.422	0.087
2 454 951.514264	166.194	0.070
2 454 964.525457	166.332	0.082
2 455 207.715279	166.330	0.074
2 455 344.525470	166.207	0.064
2 455 554.795730	166.266	0.044
2 455 620.725908	166.220	0.058
2 455 704.535965	166.112	0.045
2 456 005.692575	166.283	0.087
2 456 033.654814	166.519	0.091
2 456 033.711811	166.402	0.247
2 456 722.657147	166.376	0.152
2 457 142.537184	166.147	0.082

Table A.16. HE 1327−2326.

HJD	RV km s^{-1}	RV$_{err}$ km s^{-1}
2 454 219.542926	65.578	...
2 454 930.612715	64.974	...
2 455 232.754648	62.764	...
2 455 344.464871	63.630	...
2 455 620.712669	65.347	...
2 455 704.502164	64.463	0.935
2 455 945.751608	62.329	...
2 456 006.750000	65.188	...
2 456 796.598655	64.818	0.159

Notes. Only the spectral order containing the Mg triplet could be used for the correlation for the majority of the spectra of this star, thus an internal error could not be calculated for these spectra.

Table A.17. HE 1410+0213.

HJD	RV km s^{-1}	RV$_{err}$ km s^{-1}
2 454 219.643865	80.983	0.024
2 454 314.427327	81.213	0.028
2 454 516.758372	81.111	0.159
2 454 909.570456	81.069	0.046
2 454 930.734724	81.026	0.036
2 454 951.686449	80.874	0.028
2 455 232.768813	81.025	0.020
2 455 262.603235	80.918	0.056
2 455 344.565415	81.068	0.028
2 455 555.796783	81.291	0.178
2 455 620.765457	80.837	0.030
2 455 662.717240	80.960	0.021
2 455 704.599755	81.183	0.021
2 455 776.420181	81.414	0.016
2 456 005.703435	81.143	0.042
2 456 033.595529	81.330	0.043
2 456 078.490141	81.348	0.032
2 456 722.586745	81.417	0.173
2 457 079.771538	81.389	0.055
2 457 096.777330	81.357	0.050
2 457 110.655228	81.202	0.103
2 457 142.633878	81.069	0.031
2 457 225.423528	80.984	0.037

Table A.18. HE 1506−0113.

HJD	RV km s^{-1}	RV$_{err}$ km s^{-1}
2 456 756.666987	−85.865	1.202
2 456 796.621783	−85.830	0.153
2 456 813.637005	−83.626	0.952
2 456 893.378926	−83.223	0.594
2 457 142.677901	−81.052	0.524
2 457 190.528825	−79.152	0.449
2 457 225.469049	−77.545	0.943
2 457 239.418486	−80.405	1.765
2 457 241.405630	−80.661	0.736
2 457 249.435833	−79.985	0.798

Table A.19. CS 22878−027.

HJD	RV km s^{-1}	RV$_{err}$ km s^{-1}
2 456 191.343802	−91.097	0.810
2 456 756.724060	−89.769	0.331
2 456 796.698016	−90.696	1.839
2 456 887.392049	−90.533	1.495
2 457 142.721805	−90.845	1.446
2 457 168.690235	−92.330	1.021
2 457 225.500502	−90.822	2.506

Table A.20. CS 29498−043.

HJD	RV km s^{-1}	RV$_{err}$ km s^{-1}
2 454 314.535743	−32.557	1.583
2 454 338.491418	−32.080	0.964
2 454 373.380034	−32.911	1.247
2 454 665.594229	−32.885	1.988
2 454 705.541235	−33.060	0.421
2 455 059.460229	−32.215	1.468
2 455 070.509288	−33.641	2.553
2 455 149.322697	−31.798	1.008
2 455 415.540797	−32.527	1.318
2 455 439.469033	−32.242	1.385
2 455 738.656324	−31.819	1.760
2 455 776.589351	−32.193	0.682
2 456 033.722001	−31.172	0.865
2 456 458.700787	−32.383	1.420
2 456 917.501102	−33.836	1.839

Table A.21. CS 29502−092.

HJD	RV km s^{-1}	RV$_{err}$ km s^{-1}
2 454 314.615516	−67.045	0.061
2 454 373.458720	−67.215	0.051
2 454 625.669705	−67.200	0.061
2 454 665.647386	−67.284	0.060
2 454 705.583752	−67.143	0.054
2 454 964.724327	−67.152	0.071
2 455 059.495880	−67.266	0.065
2 455 126.513232	−67.213	0.088
2 455 174.330130	−67.225	0.055
2 455 344.673757	−67.116	0.068
2 455 415.485690	−67.193	0.066
2 455 439.439882	−67.216	0.051
2 455 503.319269	−67.452	0.088
2 455 531.397775	−67.351	0.105
2 455 704.690065	−67.173	0.082
2 455 776.526490	−67.174	0.055
2 456 139.661574	−67.368	0.066
2 456 191.367411	−67.157	0.073
2 456 458.712569	−67.180	0.068
2 456 917.518394	−67.175	0.100

Table A.22. HE 2318−1621.

HJD	RV km s^{-1}	RV$_{err}$ km s^{-1}
2 456 191.508735	−41.724	0.136
2 456 458.678220	−41.780	0.085
2 456 512.729591	−41.299	0.228
24 56 574.601390	−42.136	0.210
2 456 888.556884	−41.612	0.299
2 456 956.516288	−41.446	0.270
2 457 225.639412	−41.891	0.112

Table A.23. CS 22949−037.

HJD	RV km s^{-1}	RV$_{err}$ km s^{-1}
2 456 191.418846	−125.488	0.490
2 456 213.439688	−125.619	0.423
2 456 518.588656	−125.438	1.300
2 456 574.639061	−126.021	1.465
2 456 881.545231	−125.238	1.834
2 456 886.533402	−125.775	1.247
2 456 956.499023	−125.341	1.153

Table A.24. CS 22957−027.

HJD	RV km s^{-1}	RV$_{err}$ km s^{-1}
2 454 314.650763	−61.056	0.053
2 454 373.602779	−61.598	0.071
2 454 396.522335	−62.847	0.209
2 454 480.353018	−63.679	0.119
2 454 665.720088	−72.551	0.112
2 454 780.480070	−76.573	0.109
2 454 819.304024	−76.207	0.170
2 455 059.670725	−67.280	0.056
2 455 071.664734	−67.767	0.388
2 455 126.567510	−65.441	0.085
2 455 149.455854	−64.285	0.130
2 455 207.320651	−63.146	0.131
2 455 439.578111	−61.418	0.084
2 455 503.374442	−62.705	0.525
2 455 531.350698	−62.359	0.139
2 455 738.721957	−72.151	0.063
2 455 776.669030	−73.957	0.105
2 455 882.450486	−76.464	0.111

Appendix B: Literature data for the single programme stars

Table B.1. Mean heliocentric radial velocities from the literature and total time span covered for the single stars.

Stellar ID	ΔT total (days)	Mean RV (this work) (km s^{-1})	Mean RV (km s^{-1})	N	Ref
HE 0020−1741	3333	+93.018	+93.0	1	Kordopatis et al. (2013)
CS 29527−015	7745	+47.077	+45.7	1	Norris et al. (1996)
			+48.0	1	Aoki et al. (2013)
CS 22166−016	3727	−209.769	−210.0	1	Roederer et al. (2014)
BD+44°493	11 368	−150.084	−151.3	6	Carney & Latham (1986)
			−150.6	28	Carney et al. (2003)
			−150.3	4	Ito et al. (2013)
			−150.0	2	Roederer et al. (2014)
			−150.1	4	Starkenburg et al. (2014)
HE 1012−1540	4646	+226.362	+225.6	2	Cohen et al. (2008)
			+226.3	2	Cohen et al. (2013)
			+225.6	2	Roederer et al. (2014)
HE 1201−1512	2524	+239.450	+238.0	4	Norris et al. (2013a)
HE 1300+0157	4338	+74.536	+74.3	3	Barklem et al. (2005)
			+73.4	1	Cohen et al. (2008)
			+74.5	6	Starkenburg et al. (2014)
BS 16929−005	5157	−50.619	−51.2	1	Honda et al. (2004)
			−54.0	1	Lai et al. (2004)
			−50.4	1	Aoki et al. (2007)
			−51.7	1	Lai et al. (2008)
			−50.5	5	Starkenburg et al. (2014)
HE 1300−0641	4329	+68.822	+67.9	2	Barklem et al. (2005)
CS 22877−001	6228	+166.297	+166.1	1	Aoki et al. (2002a)
HE 1327−2326	3660	+64.344	+63.9	1	Aoki et al. (2006)
HE 1410+0213	4929	+81.140	+80.7	1	Cohen et al. (2013)
CS 22878−027	4355	−91.016	−91.3	2	Lai et al. (2008)
			−91.2	2	Roederer et al. (2014)
			−91.5	6	Starkenburg et al. (2014)
CS 29498−043	4800	−32.488	−32.5	1	Aoki et al. (2002b)
			−32.6	1	Aoki et al. (2002c)
			−32.9	3	Aoki et al. (2004)
			−32.6	2	Roederer et al. (2014)
CS 29502−092	4782	−67.215	−67.7	1	Tsangarides et al. (2003)
			−67.0	1	Lai et al. (2004)
			−65.2	1	Ruchti et al. (2011)
			−67.0	1	Sakari et al. (2013)
			−66.6	1	Roederer et al. (2014)
			−66.8	3	Starkenburg et al. (2014)
CS 22949−037	5129	−125.560	−126.4	1	McWilliam et al. (1995)
			−125.7	1	Norris et al. (2001)
			−125.6	4	Depagne et al. (2002)
			−125.6	1	Bonifacio et al. (2009)
			−125.4	2	Roederer et al. (2014)
			−125.9	2	Starkenburg et al. (2014)

References. We note that no additional radial-velocity measurements were found for HE 0405−0526, HE 1133−0555, HE 1302−0954, and HE 2318−1621.